# Supercooled Liquid β-Diketones

## with Mechanoresponsive Emission

Tristan Butler,<sup>a</sup> Fang Wang,<sup>a</sup> Margaret L. Daly, <sup>a</sup> Christopher A. DeRosa,<sup>a</sup> Diane A. Dickie,<sup>a</sup> Michal Sabat,<sup>b</sup> Cassandra L. Fraser<sup>a</sup>

<sup>a</sup> Department of Chemistry, University of Virginia, McCormick Road, Charlottesville, Virginia 22904, United States

<sup>b</sup> Department of Materials Science and Engineering, University of Virginia, 395 McCormick Road, Charlottesville, Virginia, 22904, United States

Corresponding author: <a href="mailto:fraser@virginia.edu">fraser@virginia.edu</a>

Keywords: Mechanochromism, Thermochromism, Supercooled liquid, Shear induced crystallization

#### Abstract

Shear induced crystallization of dyes in the amorphous state is an effective strategy for generating higher rather than lower energy emission after mechanical perturbation—a rare phenomenon in mechano-responsive materials. Recently, we reported that a β-diketone with a 3,4,5-trimethoxy substituted phenyl ring formed a thermally stable supercooled liquid (SCL) phase after melting and cooling in air. To tune the thermal stability of β-diketones in the SCL phase, a series of dyes with 3,4,5-trimethoxy substituted phenyl rings were synthesized. Derivatives with naphthyl and phenyl rings were prepared in order to modulate crystallization through arene interactions. Additionally, dyes were substituted with alkoxy chains of varying length to promote crystallization through increased van der Waals interactions. Video screening in conjunction with differential scanning calorimetry (DSC) and X-ray diffraction (XRD) studies indicated that naphthyl substituted derivatives exhibited increased thermal stabilities and that increasing alkoxy chain length can induce crystallization. Analysis of molecular packing for single crystals of PH, PC1, PC3, and PC5 revealed that the central para-substituted methoxy group of the trimethoxy substituted ring was forced out of the molecular plane due to steric interactions with neighboring methoxy groups. The stabilities of the SCLs were generally correlated with the torsion angles of the para methoxy groups, where derivatives with smaller angles exhibited faster rates of crystallization. Mechanical perturbation of the SCL phases resulted in shear induced crystallization for PH, PC1, PC3 and NC6 derivatives. In some cases, traditional ML with a crystalline-toamorphous phase transition was also observed, which indicates that some trimethoxy-substituted β-diketones exhibit more than one type of mechano-responsive luminescence.

#### Introduction

Luminescent materials that exhibit color changes in response to mechanical stimuli, are desirable for a variety of applications including security inks, force sensors, and optical storage devices.<sup>1–4</sup> Most of these mechanochromic luminescent (ML) materials exhibit shifts toward lower energy wavelengths after mechanical perturbation, due to crystalline-to-amorphous phase transitions.<sup>5–7</sup> In other cases, color changes are produced by mechanically generated transitions between different crystalline polymorphs.<sup>8,9</sup> For example, Ito *et al.*, have shown that arenesubstituted gold complexes can undergo crystal-to-crystal transitions with tunable emission through donor and acceptor substitution.<sup>10</sup> Systems such as these benefit from the fact that single crystal analysis can be used to probe both initial and post-smearing states.

While many reports describe ML materials with crystalline-to-amorphous phase changes, far fewer describe emission changes resulting from amorphous phases that crystallize upon smearing, with associated hypsochromic shifts. One strategy to develop these rare ML materials employs supercooled liquid (SCL) phases, where mechanical perturbation induces crystallization. For instance, Kim *et al.*, reported stimuli responsive properties of diketopyrrolopyrole (DPP) supercooled liquids. The thermal stability, triggering force, and crystallization rate were modulated by varying alkyl chain lengths which allowed for tunable properties through a balance of alkyl chain and arene interactions. In fact, when substituted with alkyl chains eight carbons in length, crystallization could be triggered by living cell attachment and cell contraction, which demonstrates its potential use as a highly sensitive force sensor. In addition to fluorescent systems, amorphous materials, such as SCLs, are also of interest for improved drug solubility, conducting materials for organic light emitting diodes (OLEDs), nanolithography, and optical memory storage. Therefore, new SCL materials may be useful for a variety of applications.

Molecules that form supercooled liquids (e.g. diphenyl hydrazone, triphenyl amine (TPA), capped oligothiophenes, and  $\pi$ -electron starburst derivatives) tend to have bulky substituents that form different non-planar conformers. As these melted molecules are cooled below their crystallization temperature, different conformations are sampled in order to reach an energy minimum and crystallize. Due to the steric bulk of these materials, efficient sampling is prevented, limiting molecular associations. Furthermore, the viscosity of the melted phase increases considerably during cooling, further hindering the molecular motion needed for crystallization.  $^{18-20}$ 

Because of their facile synthesis from commercially available starting materials<sup>21</sup> and tunable optical properties, luminescent  $\beta$ -diketones (bdks) are a particularly promising class of stimuli responsive material. Their emission properties are tunable *via* boron coordination, <sup>22</sup> alkyl chain length, <sup>23,24</sup> substituent ring size, <sup>25</sup> heavy atom<sup>26,27</sup> and donor and acceptor substitution, <sup>28,29</sup> as well as heteroatom<sup>30</sup> and steric effects. <sup>31</sup> However, the mechano-responsive emission of these materials is due to crystalline-to-amorphous phase transitions. Amorphous-to-crystalline transitions have yet to be broadly established for this class of materials. Recently we reported the ML properties of gbmOMe, a  $\beta$ -diketone with 3,4,5-trimethoxy substituted phenyl ring. In addition to rapidly recovering blue-to-green ML, we discovered that gbmOMe also forms a green emissive SCL phase after melting that is stable for up to 24 hours. <sup>32</sup> According to the crystal structure of gbmOMe, the methoxy group in the 4-postion of the trimethoxy substituted ring extends out of the plane of the molecule which may provide the steric bulk needed for the formation of the SCL state. Hence, synthesizing other molecules with this motif may be an effective design strategy to form SCL phases in a predictable fashion.

Inspired by the design strategy of Kim *et al.*,<sup>11</sup> a series of trimethoxyphenyl bdks were synthesized, incorporating phenyl and naphthyl rings to probe arene effects on the thermal stability of supercooled liquid phases (Figure 1). Additionally, both sets of dyes (phenyl and naphthyl) were substituted with alkoxy groups of varying alkyl length (n = 0, 1, 3, 5, 6, 12) in order to induce van der Waals interactions and drive crystallization. Previous reports of alkyl chain length and arene size effects on the mechanochromic luminescence (ML) of BF<sub>2</sub>bdk materials indicate that the stimuli responsive optical properties of spin-cast films (e.g. thermal, ML) may be affected in addition to the thermal stability of supercooled liquids.<sup>23,24</sup> Thermal and structural characterization of these dyes was performed using differential scanning calorimetry (DSC) and X-ray diffraction (XRD), respectively. When possible, single crystals were grown and assessed by XRD to provide insight into the intermolecular and packing interactions that influence the thermal stability of the melted phase. Solid-state optical properties, including shear-induced crystallization, were investigated for bulk powders and melted films. Additionally, thin films were fabricated in order to investigate the ML response of each dye.

**Figure 1.** Chemical Structures of Diketones. Dyes are named for the arene ring (P = phenyl, N = naphthyl) and the length of the alkyl chain (e.g. C1 = methyl, C3 = propyl). For example, PC1 is a phenyl dye with a methoxy substituent.

## **Experimental Section**

Materials

THF was dried over molecular sieves activated at 300 °C as previously described.<sup>33</sup> Reactions were monitored using silica TLC plates. Compounds purchased from Sigma-Aldrich and TCI were reagent grade and used without further purification. The trimethoxy-substituted β-diketones were synthesized *via* Claisen condensation using a previously described method.<sup>34</sup> Williamson ether synthesis was used to prepare alkoxy-substituted ketone building blocks using a previously described method.<sup>34</sup> Data for PH<sup>35</sup> and PC1<sup>35</sup> are in accord with previous reports.

### Methods

<sup>1</sup>H NMR (600 MHz) spectra were recorded on a Varian VRMS/600 spectrometer in deuterated DMSO. Spectra were referenced to the signals for residual protio-DMSO at 2.50 ppm or protio-CDCl<sub>3</sub> at 7.24 ppm. The coupling constants for each compound were reported in Hz. Mass spectra were recorded using a Micromass Q-TOF Ultima spectrometer, using electrospray ionization (ESI) MS/MS techniques. Absorption spectra were collected on a Hewlett-Packard 8452A diode-array UV-vis spectrophotometer and a Horiba Fluorolog-3 Model FL3-22 spectrofluorometer (double-grating excitation and double-grating emission monochromator) was used to measure steady-state emission spectra. Time-correlated single-photon counting (TCSPC) fluorescence lifetime measurements were obtained with a NanoLED-370 ( $\lambda_{ex} = 369$  nm) excitation source and a DataStation Hub as the SPC controller. Analysis of lifetime data was performed using DataStation v2.4 software from Horiba Jobin Yvon. Fluorescence quantum yields, φ<sub>F</sub>, in CH<sub>2</sub>Cl<sub>2</sub> were calculated versus a standard of dilute quinine sulfate solution in 0.1M H<sub>2</sub>SO<sub>4</sub> using a previously described method<sup>36</sup> and the following values:  $\phi_F$  quinine sulfate in 0.1M H<sub>2</sub>SO<sub>4</sub> =  $0.54,^{37}$   $n_D^{38}$  0.1M  $H_2SO_4 = 1.33$ ,  $n_D^{38}$   $CH_2Cl_2 = 1.424$ . Optically dilute  $CH_2Cl_2$  solutions (absorbances <0.1 AU) of all samples were prepared in 1 cm path length quartz cuvettes. To measure the solid-state quantum yields, a F-3029 Quanta-Φ Integrating Sphere from Horiba Scientific was utilized and data were analyzed using FluorEssence software. A Laurel Technologies WS-65OS spin-coater was used to fabricate thin films for mechanochromic testing. Differential scanning calorimetry (DSC) was performed on the pristine powders using a TA Instruments 2920 Modulated DSC. Data were analyzed using the Universal Analysis Software V 2.3 from TA Instruments. Thermograms were recorded using the standard mode and a constant heating rate of 5 °C/min. A cooling rate of 10 °C/min was used during the initial cycle compared to a cooling rate of 1 °C/min for subsequent cycles. Powder x-ray diffraction (XRD) patterns were obtained using a Panalytical X'Pert Pro MPD diffractometer operating at 40 kV and 40 ma using Cu Kα radiation.

Single Crystal Analysis. Single crystals of PH, PC3, and PC5 for XRD analysis were grown by vapor diffusion of hexanes into concentrated THF solutions. The crystallographic data for PC1 was previously reported.<sup>32</sup> Data sets were obtained using a Bruker Kappa Duo CCD diffractometer at -120 °C using Mo Kα radiation. Data obtained from single crystal XRD was analyzed with Mercury 3.9 software from the Cambridge Crystallographic Data Centre. Crystal data of PH follow the monoclinic space group P21/c, a = 7.3484(10) Å, b = 22.855(3) Å, c = 9.6250(13) Å, β = 102.525(2) °, Z = 4, V = 1578.0(4) Å<sup>3</sup>. The structure was solved using the charge flipping method in Bruker SHELXTL program and refined to R = 0.0523 using 6683 reflections with  $I > 2\sigma(I)$ . Crystal data of PC3 follow the monoclinic space group P21/n, a = 9.1276(6) Å, b = 15.3317(10) Å, c = 13.5716(9) Å, β = 102.751(1) °, Z = 4, V = 1852.4(2) Å<sup>3</sup>. The structure was solved using the charge flipping method in Bruker SHELXTL program and refined to R = 0.0627 using 7538 reflections with  $I > 2\sigma(I)$ . Crystal data of PC3 follow the triclinic space group P-1, a = 10.8234(16) Å, b = 10.8522(16) Å, c = 18.235(3) Å, β = 92.755(3) °, Z = 4, V = 2087.6(6) Å<sup>3</sup>. The structure

was solved using the charge flipping method in Bruker SHELXTL program and refined to R = 0.0922 using 11053 reflections with  $I > 2\sigma(I)$ .

Preparation of Thin Films. Spin cast films for ML analysis were made by applying 20 drops of a dye stock solution in dichloromethane (0.018 M) to microscope coverglass rotating at 3000 rpm. Samples were dried under vacuum for 20 min prior to annealing phenyl and naphthyl derivatives at 75 °C and 85 °C respectively, for 10 min. In most cases, green emission remained after annealing, so films were gently smeared with a Kimwipe, followed by annealing again at 75 °C (phenyl) or 85 °C (naphthyl) for another 10 min to produce uniform blue emission. Mechanical perturbation of films was performed through gentle smearing with a cotton swab. Films for video analysis and emission measurements of melted and crystalline phases were fabricated by adding dye (~ 50 mg) to microscope coverglass and melting using a hot plate. Once melted, films were immediately removed from the hot plate for air cooling to room temperature. Shear induced crystallization properties were investigated by rubbing films with a wooden applicator repeatedly, for up to 2 min or until a color change was observed.

Video Analysis. Videos were recorded at room temperature using a PGR GS3-U3-41C6C-C video camera with a complementary metal oxide semiconductor CMOS chip capable of 90 frames per second (FPS) at a maximum resolution of 2048x2048 pixels. The camera was also equipped with a Spacecom f/0.95 50 mm lens and an Edmund Optics 425 nm long pass filter to minimize excitation background. The camera was operated with a Lenovo W530 laptop connected via a USB 3.0 cable. Point Grey FlyCap2 software was used to record videos of films. The camera was placed approximately 0.5 m above the sample, which was illuminated with a 100W Black-Ray B-100AP/R lamp at 365 nm located ~10 cm above the sample.

#### **Results and Discussion**

## Synthesis

In order to investigate the stability of supercooled liquid states and ML properties of β-diketone dyes, a series of phenyl (Scheme S1) and naphthyl (Scheme S2) derivatives was synthesized via Claisen condensation with the appropriate ketone/ester pair. The ketone starting materials for both phenyl and naphthyl derivatives were synthesized *via* Williamson ether synthesis using a previously described method.<sup>34</sup> Diketones were soluble in common organic solvents (e.g. CH<sub>2</sub>Cl<sub>2</sub>, THF, CHCl<sub>3</sub>), however solubility in hexanes varied depending on the length of the alkoxy chain. That is, longer chains corresponded to greater hexane solubility. Peaks near 17.0 ppm were observed in the NMR spectra for all dyes, which indicates the enol form is present in solution.

## Optical Properties in Solution

The optical properties of the dyes were measured in dilute ( $10^{-5}$  M) dichloromethane solutions (Figure S1, Figure S2, Table S1). As a result of increased conjugation, redshifted absorption and emission were observed for naphthyl derivatives versus phenyl dyes. With the exception of the hydrogen-substituted derivatives that were slightly blue shifted compared to other dyes, little deviation in peak absorbance ( $\lambda_{abs}$ ) was detected within each set of dyes (i.e. phenyl, naphthyl). As expected and previously observed, alkoxy substitution results in red-shifted emission due to increased electron donation versus H, however alkyl chain length has little effect on absorption.<sup>23</sup> All dyes exhibited similar molar absorptivities ranging from 55000 for NC3 to 81000 for NC5 regardless of phenyl or naphthyl substitution. Typically, increasing conjugation results in larger absorbing cross-sections and increased molar absorptivity, however no such trend was observed

for these trimethoxy dyes. One potential explanation could be that twisting of arene rings in the ground state limits the absorbing cross-section of both sets of dyes.<sup>31</sup>

Visual inspection of UV excited samples indicated that dyes are essentially non-emissive in solution, further evidenced by low quantum yields ( $\phi$  < 3%) irrespective of increased conjugation or alkoxy substitution. Similar to their absorption in solution, the emission of naphthyl dyes was redshifted compared to phenyl substituents via fluorescence spectroscopy. Phenyl derivatives PH and PC12 show redshifted emission compared to other derivatives of this kind. Similarly, no trends in emission with alkyl chain length could be established for naphthyl dyes. Relatively short lifetimes (< 0.5 ns) were observed for both sets of dyes, which is consistent with other bdk derivatives (e.g. bromo and methoxy dinaphthoylmethane (dnm) dyes; < 0.23 ns;<sup>22</sup> and 3,4,5,-trimethoxy derivatives with fluoro, iodo, and cyano substituents: < 0.23 ns).

## Video Characterization of Melted Films

Qualitative screening of the thermal properties for blue-emissive bulk powders indicated that all dyes form a green-emissive melted phase, however the duration of the melted phase was dependent on the presence and length of the -OR group. In order to compare the stability of the melted states and probe mechanical shearing effects, videos were recorded of melted diketone thin films (Figure 2). Films of the melted state were prepared by adding a small amount of dye (~20 mg) to a microscope slide followed by heating on a hotplate. Once the dye melted, it was spread evenly across the microscope slide using a wooden applicator. Videos were recorded immediately after removal from the heat source, but the duration of the video depended on the stability of the melted phase. For films that exhibited phase changes (i.e. formation of blue-emissive species) without mechanical perturbation, videos were recorded until the melted phase disappeared (i.e. the absence of green emission from the SCL/melt). If no blue phase was detected after 10 min or

longer, films were sheared vigorously using a wooden applicator and videos were recorded for up to three hours in order to monitor mechanically induced phase changes.

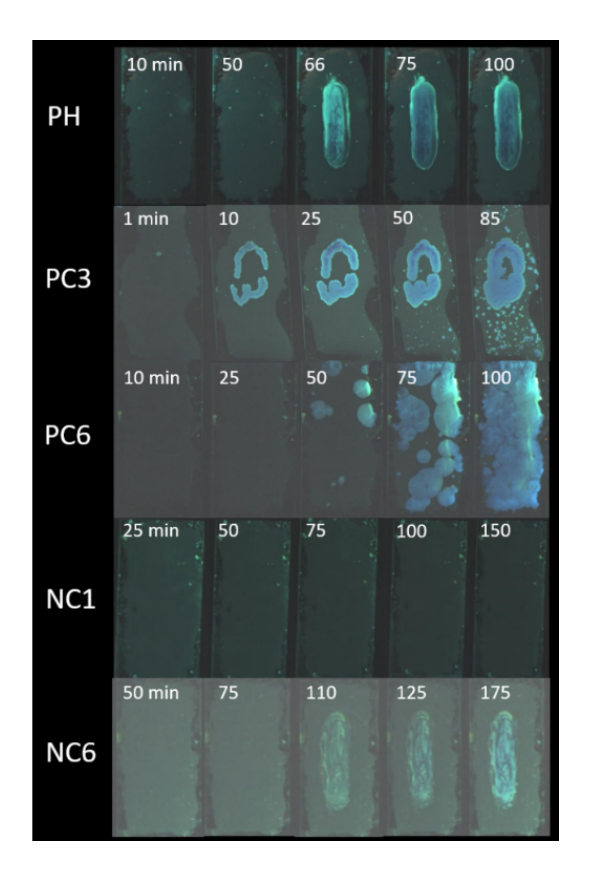


**Figure 2**. Video frames demonstrating the effect of alkoxy substitution on the thermal stability and shear induced phase changes of phenyl and naphthyl substituted diketone supercooled liquids/melts. Mechanical perturbation was applied to PH, PC3, NC1, and NC6 in order to induce crystallization. For PC6, spontaneous crystallization was observed after melting so that sample was not smeared.

As with initial observations, videos indicated that the thermal stability of the melted phase of phenyl dyes is correlated with the length of the alkoxy chain. For PC12, the dye with the longest chain, a transiently stable (~1 min) melted phase with green emission was initially formed before rapidly turning blue. Dyes with intermediate chain lengths, PC5 and PC6, formed green emissive melted states that were stable for several minutes, however blue emissive regions eventually begin to form without mechanical stimulus (Figure 2, PC6). The stability of the melted phase was much greater for dyes with shorter (≤ 3 carbon atoms) alkoxy chains. The PC3 dye formed a green phase

when melted but slowly transitioned to the blue phase over approximately three hours. The emergence of the blue emissive phase in PC3 can be expedited through mechanical perturbation, as gentle smearing of the relatively fluid melted phase resulted in the rapid appearance of blue emission. As described in a previous report, melted PC1 films were thermally stable for several hours before crystallization occurred, however the effect of mechanical smearing on the melt phase was not investigated.<sup>32</sup> While smearing resulted in a localized phase change, compared to PC3, repeated smearing was required in order to generate blue emissive PC1 films. Additionally, the transition was not immediate, as a significant period of time (i.e. 15 min) elapsed between mechanical smearing and the observation of blue emission. The most stable melted phase was measured for PH films which still showed green emission after 24 hours. Vigorous smearing of these films resulted in the emergence of localized blue emission. Though PH was harder to smear than PC3, it was much less viscous than PC1 films and also exhibited a more rapid phase change after smearing (i.e. 1 min).

Naphthyl dyes also formed stable amorphous phases when melted and quenched in air. After initial cooling, NC3 and NH formed thermally stable melts that were brittle and difficult to smear, whereas the melted phase of NC1 was more fluid by comparison. Like its phenyl counterpart, NC12 formed a green emissive melt that rapidly converted to a solid blue-shifted phase after a few minutes. All other naphthyl substituted dyes form melted phases that are stable for over 24 hours regardless of –OR substitution. Inspection of the films after two days, showed that blue emissive phases eventually encompassed the entire film. For NC6, a localized phase transition was induced through vigorous smearing of the relatively viscous melted phase, however, for the other naphthyl films at room temperature, application of mechanical stimulation did not induce any phase changes. However, phase changes localized to smeared regions could be

produced after smeared films were gently heated. Differences in viscosity were observed depending on alkoxy substitution and chain length.

In summary, the stabilities of the melted phases were longer for naphthyl versus phenyl dyes. One potential explanation for this is that increased arene-arene interactions result from naphthyl substitution, and materials form species at a local energy minimum, thereby preventing transition to a different phase. In support of this assertion, previously we have seen lower solubility and increased aggregation at lower concentration for naphthyl versus phenyl dyes. 99,40 Furthermore, this study indicates that the stability of melted phases for both phenyl and naphthyl derivatives were tunable based on alkoxy chain length, as the melted phases for C12 substituted dyes exhibited much lower melt stability (i.e. shorter melt lifetimes) compared to other phenyl and naphthyl diketones. Phenyl dyes were more sensitive to alkyl chain length effects, as PH, PC1, and PC3 showed progressively less stable melted phases, whereas highly stable melted phases were noted for corresponding naphthyl films. Additionally, phenyl derivatives showed greater propensity for mechanically induced phase changes since PH, PC1, and PC3 all formed blueshifted phases after smearing, but NC6 was the only naphthyl derivative that formed a blue emissive phase at room temperature after mechanical perturbation.

## Powder XRD Characterization of Melted Thin Films

Screening of thermal responses indicated that dyes existed as transparent green emissive melted states that, in some instances, transitioned to opaque solids with brighter and higher energy emission. To better understand the identity and structural factors associated with these phases, powder x-ray diffraction (XRD) patterns were measured for dyes as bulk powders and melts (Figure 3, Figure S3).

Analysis of powder patterns for phenyl dyes indicated that derivatives with shorter alkyl chains (< C6) were crystalline as bulk powders, but mostly amorphous as thin films that were melted and then cooled to room temperature. With the exception of PC3, no diffraction peaks were observed in the powder patterns of the melted films for these dyes, which indicates that they are amorphous. For PC3, small peaks were observed in the melted phase which may be due to the formation of small crystalline regions during the course of the measurement. The XRD patterns for bulk powders and melted films of phenyl dyes with longer alkoxy chains, PC6 and PC12, indicated that both states were populated with crystalline species. Therefore, melted PC6 and PC12 films rapidly converted to a crystalline blue-emissive phase which is consistent with video characterization. Comparison of the bulk powder and melted patterns of PC6 shows that the same crystalline phase is present in both states, whereas the XRD data for PC12 shows several peaks in the bulk powder pattern that are absent when melted and crystallization occurs afterwards. This suggests that multiple crystalline phases are present in the bulk powder of PC12, some of which were not formed when PC12 was melt quenched.

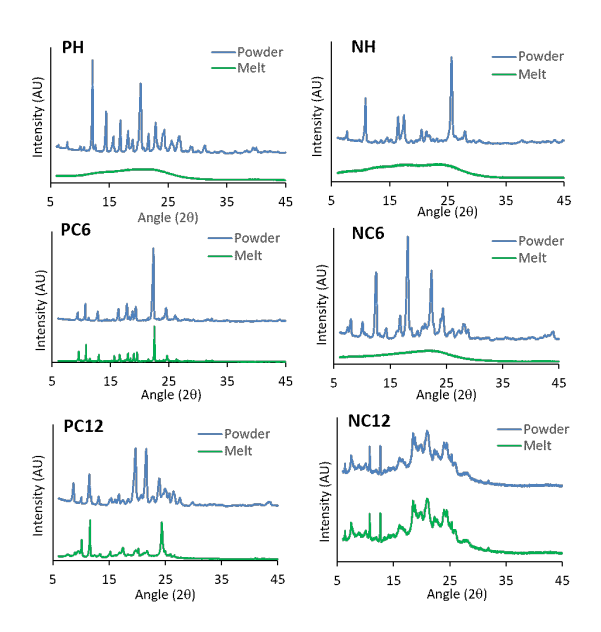


**Figure 3**. Powder X-ray diffraction patterns of selected phenyl and naphthyl dyes as powders and melted films.

The XRD patterns of bulk powders and melted films of naphthyl compounds showed similar behavior to their phenyl counterparts. With the exception of NC12, all dyes exhibited crystalline powder phases, and no peaks were observed after melt quenching, thereby demonstrating that the melted phases formed by naphthyl dyes are amorphous. Similar to PC12, melted NC12 films form a crystalline phase after cooling however it is comprised of the same crystalline species as the corresponding bulk powder. These results are similar to previous investigations of the thermal response of heteroarene BF<sub>2</sub>bdks and dimethylamino diketones, as amorphous phases were also formed after melt quenching.<sup>28,30</sup>

### Single Crystal Analysis

Homogeneous nucleation theory asserts that the crystallization behavior of melted dyes can be limited by nucleation of molecules as well as propagation of crystallites.<sup>41</sup> These properties can be affected by intermolecular and solid-liquid interfacial interactions, in addition to the ability of molecules to sample different conformations.<sup>19</sup> The intermolecular interactions and dye conformations that are experienced by dyes as solids not only provide insight into their crystallization dynamics, but also determine their optical properties. In order to analyze the intermolecular contacts that control the crystallization of trimethoxy diketones, single crystal XRD was employed. Attempts were made to grow crystals of all dyes, and PH, PC3, and PC5 formed crystals suitable for diffraction. The solid-state conformations (Figure 4, Figure S4) and packing interactions (Figure 5, Figure S5) were investigated for these dyes and compared to PC1, which has been reported previously.<sup>32</sup> For clarity, different colors were used to denote dyes of the same orientation (Figure 5). Single crystals of PH, PC3, and PC5 were grown by vapor diffusion of hexanes into concentrated THF solutions. Regardless of alkoxy substituent, all dyes crystallized into block-like structures that exhibited blue-green emission under UV irradiation. The

corresponding emission spectra were similar to their bulk powders, which suggests that similar species are present in both forms (Figure S6).

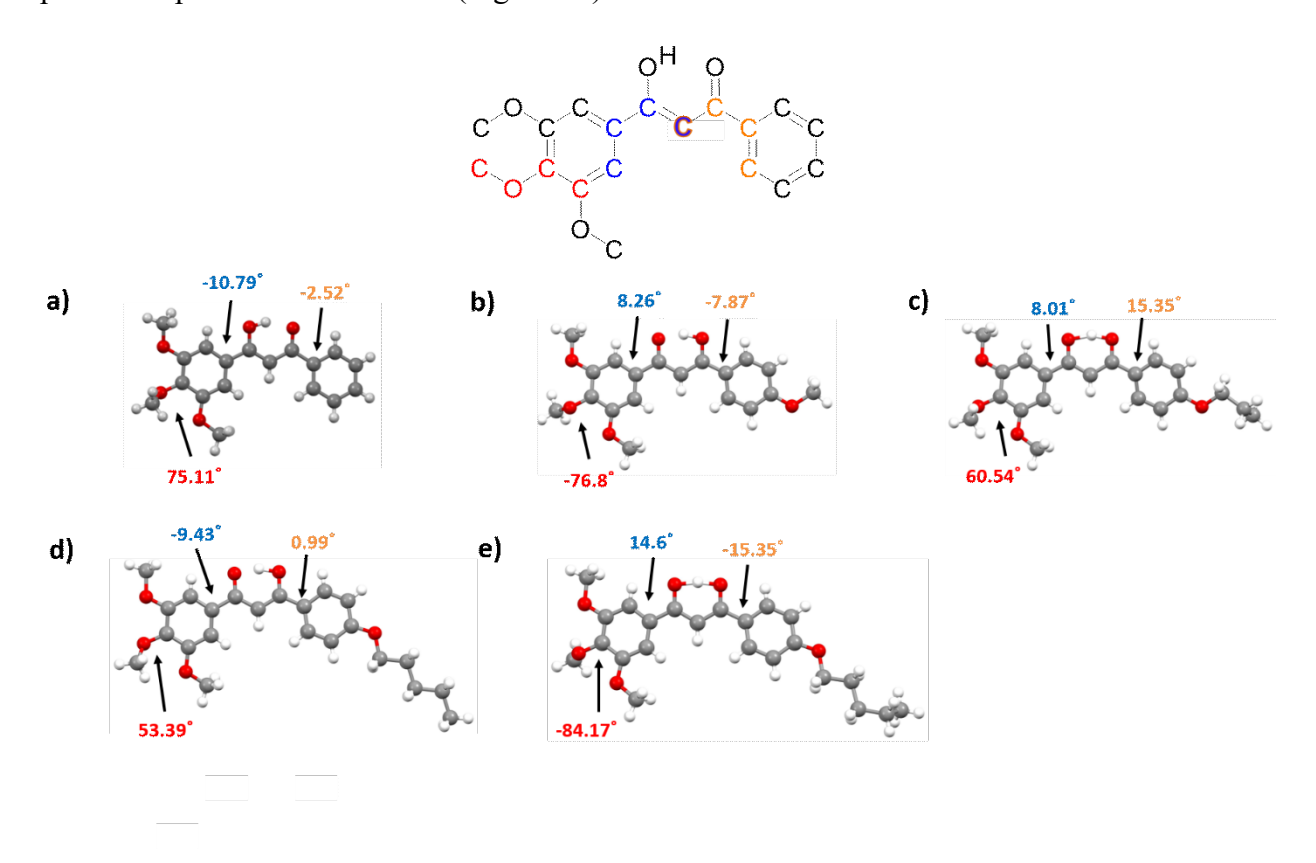


**Figure 4**. Single crystal structures highlighting selected torsion angles of PH (a), PC1 (b), PC3 (c)  $\alpha$ -PC5 (d) and  $\beta$ -PC5 (e).

Examination of the solid-state conformation of PH shows that the para-substituted methoxy group is directed out of the plane of the molecule, which has previously been attributed to steric interactions between neighboring methoxy substituents.<sup>32</sup> The torsion angle between the phenyl ring and this methoxy substituent (∠C12 C13 O4 C17 = 75.11°) shows that it is nearly orthogonal to the molecular plane. Additionally, the trimethoxy phenyl ring of PH was slightly twisted relative the plane of the molecule. Based on the respective torsion angles, the methoxy-substituted ring deviates from planarity more than the unsubstituted ring, which also may be attributable to steric interactions. The unit cell of PH indicates that dyes assembled with O-C-H···arene interactions

between the para-substituted methoxy group on the trimethoxy ring of one dye and the same arene ring of an adjacent molecule. Additionally, multiple C=O···H-C interactions are noted between aryl hydrogens of the unsubstituted ring and the methine group of the ketone/enol core. Though intramolecular hydrogen bonding can be observed in the enol moiety, no intermolecular hydrogen bonding interactions between PH molecules were observed. Crystal packing of PH reveals that molecules crystallized into an interlocking series comprised of dyes with the same orientation offset with respect to each other. The closest arene-arene distance was estimated by measuring the distance between trimethoxy ring centroids of blue/red (4.979 Å) and green/yellow (5.181 Å) PH dyes. These distances are relatively long and are indicative of the lack of  $\pi$ - $\pi$  interactions within the crystal structure. The out-of-plane methoxy groups on neighboring molecules are directed towards each other and may prevent close associations of arene groups.

The crystal structure of PC1 was previously reported and the results are summarized here for comparison.<sup>32</sup> Briefly, the single crystal of PC1 shows the dye is mostly planar, however the methoxy group extends out of the plane of the molecule. The torsion angle associated with the out-of-plane methoxy substituent and arene ring of PC1 ( $\angle$ C6 C7 O4 C17 = -76.8°) is nearly orthogonal compared to corresponding angles in PH crystals. According to its crystal packing, PC1 dyes stack in a herringbone type motif and the crystal is characterized by C-H···O-C, C-H···H-arene and C=O··H-C interactions (Figure 5). The intermolecular distance of PC1 was measured between centroids assigned to the trimethoxy-substituted ring of blue oriented dyes and the mono substituted arene ring of PC1 dyes in the yellow orientation (3.765 Å). These centroids were chosen in order to examine arene groups in the closest proximity. While this distance is shorter than in the PH derivative, it is still too long for  $\pi$ - $\pi$  interactions. Compared to PH, where the out-of-plane methoxy groups of neighboring dyes were opposed each other, the methoxy groups of

PC1 dimers point in the same direction, and the molecules of PC1 where slightly offset with respect to one another. The alleviation of steric interactions of opposing methoxy groups and the offset conformation of PC1 dye molecules could lead to the closer packing arrangement observed for PC1.

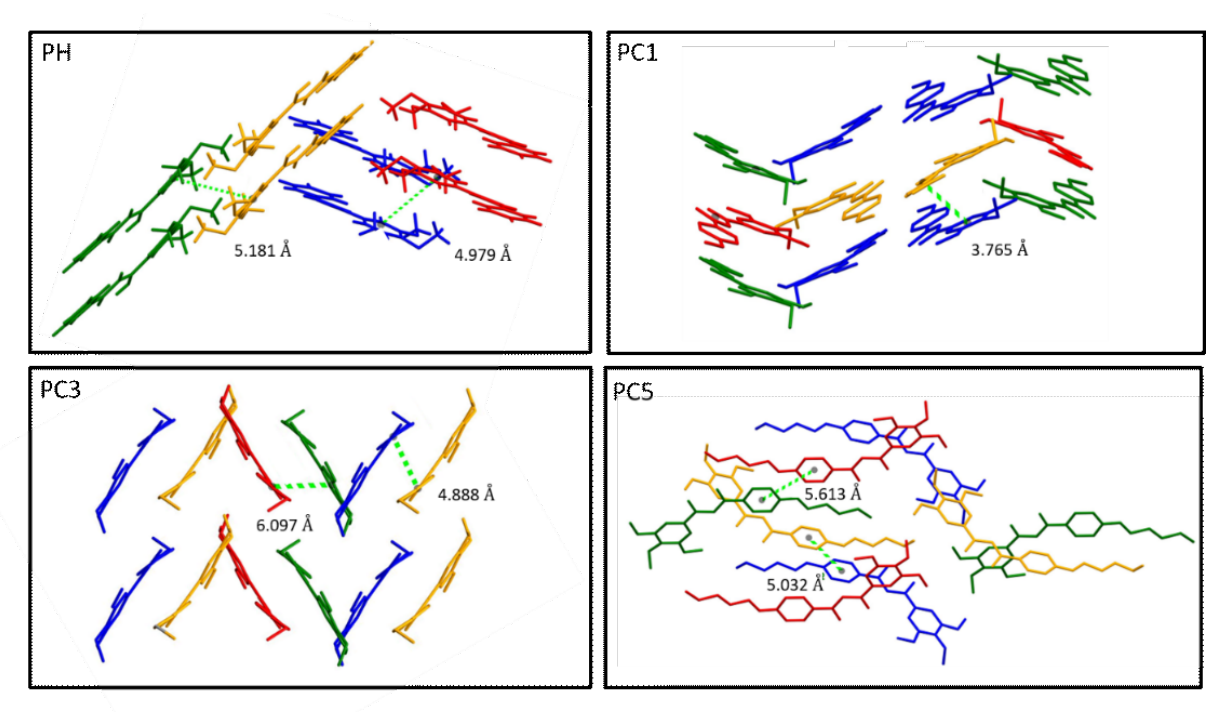


**Figure 5**. Crystal packing of selected trimethoxy diketones. For clarity in molecular packing figures, dyes are assigned different colors depending on their orientation. Additionally, hydrogens are omitted for clarity for PC1, PC3, and PC5. Two molecular conformations ( $\alpha$ -PC5 and  $\beta$ -PC5) exist in the unit cell of PC5.

As with PH and PC1, the single crystal structure of PC3 exhibited a mostly planar conformation, but phenyl rings were slightly twisted with respect to each other. However, the C3 substituted ring was slightly more twisted ( $\angle$ C3 C4 C5 C9 = 15.35°) with respect to the ketone/enol core than both PH and PC1. This may be the result of unfavorable steric interactions generated by the kinked C3 chain, which points below the molecular plane. While, PC3 also shows an out-of-plane methoxy group ( $\angle$ C15 C16 O5 C20 = 60.54°), the torsion angle is smaller than those measured for PH and PC1 structures. Furthermore, it is directed above the plane of the molecule

whereas the opposite was observed for dyes with shorter alkoxy chains. According to the unit cell of PC3, C-O···H-C interactions from trimethoxy substituted rings, and C=O···H-C contacts, which originate from separate molecules, both associate with the C3 chain of the same neighboring dye. Like the other derivatives, no hydrogen bonding or  $\pi$ - $\pi$  interactions were observed. The herringbone-type packing arrangement of PC3 shows that dyes are arranged in an interlocking series of equivalent, but offset dimers. The inter-dimer distance was estimated by calculating the distance between centroids for trimethoxy substituted rings of dyes in blue/yellow pairs (4.888 Å), and between centroids of trimethoxy substituted and mono substituted rings of different molecules (red/green pairs, 6.097 Å). The difference between distances is further demonstration that dyes are offset and that distances are too long for  $\pi$ - $\pi$  interaction.

Unlike the other crystals, PC5 exists as two different molecular conformations in the unit cell ( $\alpha$ -PC5 and  $\beta$ -PC5). For both molecules, para-substituted methoxy substituents were out of plane with respect to the molecule, however when in the same orientation, the methoxy group of  $\alpha$ -PC5 was directed above the plane of the molecule whereas the corresponding methoxy group of  $\beta$ -PC5 pointed below. The torsion angle for this group in  $\alpha$ -PC5 ( $\angle$ C46 C41 O11 C45 = 53.39°) was smaller than  $\beta$ -PC5 ( $\angle$ C11 C18 O5 C22 = -84.17°) and other trimethoxy derivatives. In addition to differences in the para-substituted methoxy group, the alkoxy chain for  $\alpha$ -PC5 was planar compared to  $\beta$ -PC5, which showed a kinked chain with the terminal carbon extended below the molecular plane. While the trimethoxy-substituted ring was out of plane for both  $\alpha$ -PC5 and  $\beta$ -PC5, the mono substituted ring of  $\alpha$ -PC5 was mostly planar ( $\angle$ C25 C26 C27 C32 = 0.99°), similar to the corresponding alkoxy chain, and  $\beta$  was twisted out of the plane of the molecule ( $\angle$ C2 C3 C4 C9 = -15.35°).

The unit cell of PC5 shows C=O···H-Ar interactions between the ketone/enol core of  $\alpha$ -PC5 and arene groups of  $\beta$ -PC5 dyes. Additionally,  $\alpha$ -PC5 dyes show O-C-H···H-C contacts between the trimethoxy substituted ring of  $\beta$ -PC5 and the alkoxy chain of  $\alpha$ -PC5, however no intermolecular associations were noted for the alkoxy group of  $\beta$ -PC5. The lack of interaction with the alkoxy chain of  $\beta$ -PC5 may explain its kinked structure. Molecular packing of PC5 shows herringbone-type packing with dyes stacked at angles to each other, which indicates that PC5 dimers are not formed. Inter-arene distances were estimated by measuring the distances between centroids of alkoxy substituted rings in red and green (5.613 Å) molecular pairs, and for  $\alpha$ -PC5 and for blue and yellow (5.032 Å) conformations which represent  $\beta$ -PC5. Large distances were observed between arene groups for both arrangements, consistent with the absence of  $\pi$ - $\pi$  interactions.

Comparison of crystal data shows that the introduction of alkoxy groups with increasing chain lengths greatly effects dye conformation and packing of phenyl derivatives. While the packing of each dye varied significantly with the alkoxy chain, several similarities were also noted. For example, no  $\pi$ - $\pi$  or hydrogen bonding interactions were observed for any of the dyes, and only C-O···H-C and C-H···H-C interactions were detected. Additionally, phenyl rings were twisted with respect to ketone/enol core and the para-substituted methoxy group of the trimethoxyphenyl ring was directed out of the molecular plane for all dyes, including both conformations of PC5. These similarities can give insights into the thermal stability of the amorphous phase.

According to homogeneous nucleation theory, the rate of nucleation, and the rate of propagation determine crystal growth. In particular, the nucleation of dyes is governed by the intermolecular interactions in the crystal. It has been proposed previously that the out-of-plane methoxy substituent may prevent dye nucleation and therefore crystallization. Comparison of the

torsion angles of methoxy groups shows that the increased thermal stability of the amorphous state is observed for dyes when torsion angles are closer to 90° or orthogonal to the plane of the molecule. For PH, the dye with the longest lived amorphous state, the para-substituted methoxy group was out of plane. Furthermore, neighboring dimers show methoxy groups directed towards each other. These interactions could prevent molecular associations and likely increase stability of the amorphous phase. The crystal structure of PC1 showed a large torsion angle, however out of plane methoxy groups were stacked in same direction which could ease steric interactions compared to PH. Modest torsion angles were observed for PC3, and methoxy groups were pointed in opposing directions, which allows for greater dye-dye interactions and limit stability of the melted phase.

Video characterization revealed that the thermal stability of melted PC5 films was shorter compared to other dyes with attainable crystal structures, but the different conformations of PC5 in the unit cell show different torsion angles between molecules. The  $\alpha$ -PC5 derivative exhibits the smallest torsion angle of all single crystals, and may allow for dye-dye interactions. Conversely, the torsion angle of the para-substituted methoxy group of  $\beta$  dyes was nearly orthogonal, and could prevent dye associations. However, the unit cell of PC5 shows interactions between ketone/enol core and C5 chain which could facilitate nucleation, and limit stability of the amorphous state. In conjunction with qualitative screening of trimethoxy substituted dyes, these crystal structures provide insight into the structural interactions that govern the thermal stability of the amorphous state tunable via alkoxy substitution.

### Thermal Properties

The ease with which dyes access different conformations in a liquid is a determining factor in the crystallization dynamics of a given material. This is related to the viscosity of the liquid

phase and is therefore highly temperature dependent. <sup>18,19,42</sup> Additionally, substituent effects such as alkoxy and arene substitution have been shown to induce viscosity changes as well as promote van der Waals interactions, which can be used to tune stability of melted phases. <sup>11</sup> Previous investigations of the thermal properties of PC1 indicated that a supercooled liquid phase was formed when melted PC1 films were cooled in air. Thermal characterization of the supercooled liquid phase was performed using differential scanning calorimetry (DSC) with variable cooling rates. If cooled sufficiently slowly, an exothermic peak indicative of crystallization was observed, however no peaks were detected when PC1 was cooled rapidly, indicating formation of a supercooled liquid phase. In order to probe the effect of alkoxy chain length and arene size on the phase transitions produced by heating, successive DSC thermograms were gathered for each dye with variable cooling rates. For the first cycle the dyes were cooled rapidly (10 °C/min), followed by slow cooling (1 °C/min) in order to facilitate crystallization when possible (Table 1).

The dependence of crystallization on cooling rate for these molecules indicates that some dyes adopt a supercooled liquid phase when rapidly cooled. Furthermore, comparison of thermograms for selected phenyl dyes (Figure 6, Figure S7) shows that alkyl chain length affects the stability of the supercooled liquid, in accordance with video studies. Examination of thermal properties for the first cycle shows that most phenyl dyes melt at similar temperatures ( $T_m \sim 100$  °C), however PC1 ( $T_m = 112.4$  °C) and PC3 ( $T_m = 123.6$  °C) exhibited slightly higher melting points. Crystallization transitions were observed in the first cooling cycle for phenyl dyes with alkoxy chains longer than three carbons. If unsubstituted or substituted with shorter alkoxy chains (PH, PC1, PC3), no exothermic transitions were noted after rapid cooling, indicative of supercooled liquid states.

**Table 1**. Thermal Properties or Trimethoxy-Substituted Diketones.

	Cyc	<b>ele</b> 1 <sup>a</sup>	Cycle 2 <sup>b</sup>				
	$T_m^{c}$	$T_c^{d}$	$T_m^{c}$	$T_c^{d}$			
PH	101.5	-	-	-			
PC1	112.4	-	116.5	-			
PC3	123.6	-	121.5	54.1, 90.8, (84.2)			
PC5	105.4	(62.3)	104.3	(69.6)			
PC6	98.5	(41.6)	97.4	(65.5)			
PC12	95.2	(63.0)	94.7	(78.1)			
NH	89.5	-	-	-			
NC1	134.1	-	133.3	102.5, (107.5)			
NC3	116.3	-	114.4	87.5			
NC5	102.0	-	101.6	78.9			
NC6	120.1	-	119.2	67.0, (94.3)			
NC12	77.0	(42.9)	79.6	43.4, (44.6)			
a TT - 41		10.00/:		4 10 00/			

<sup>&</sup>lt;sup>a</sup> Heating rate: 10 °C/min, Cooling rate: 10 °C/min

During the second heating cycle, exothermic transitions attributable to crystallization were observed for PC1 and PC3. Most dyes also exhibited melting points similar to those in the first cycle, but no crystallization or melting transitions were noted for PH. This indicates that nucleation/growth of crystals was not induced even after heating. Based on the crystal structure of PH, steric hindrance from opposing para-substituted methoxy groups may prevent crystallization. Two exothermic transitions were observed for PC3, which suggests that multiple phases were formed during rapid cooling of PC3. Slow cooling resulted in an exothermic crystallization transition for PC3 ( $T_c = 84.2$  °C), however no peaks were observed for PC1 and PH even after slow cooling. Slow cooling of dyes with longer alkyl chains (>3) resulted in higher crystallization temperatures on the second cycle.

<sup>&</sup>lt;sup>b</sup> Heating rate: 10 °C/min, Cooling rate: 1 °C/min

<sup>&</sup>lt;sup>c</sup> Melting point given in <sup>c</sup>C as the peak of the major endothermic transition.

<sup>&</sup>lt;sup>d</sup> Crystallization temperatures given in <sup>o</sup>C as the peak of exothermic transitions. Transitions reported in parenthesis occurred during the cooling phase of each cycle.

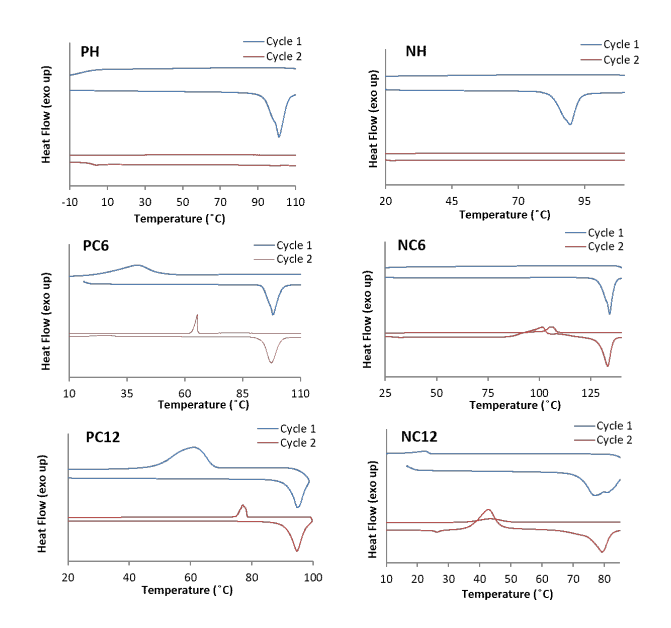


**Figure 6**. Differential scanning calorimetry (DSC) thermograms of selected phenyl and naphthyl substituted dyes (heating rate: 5 °C/min) cooled at different rates (Cycle 1: 10 °C/min; Cycle 2: 1 °C/min).

Compared to phenyl dyes, a greater range of melting temperatures was observed for naphthyl dyes (Figure 6, Figure S7). The lowest melting temperature was measured for NC12 ( $T_m = 77.0 \, ^{\circ}$ C) whereas NC1 ( $T_c = 134.1 \, ^{\circ}$ C) melted at the highest temperature relative to all other dyes. Similar to their phenyl counterparts, no exothermic transitions were observed for NH, NC1, and NC3 on the first cooling cycle, however crystallization peaks were not observed upon reheating of NH. Like PH, this indicates that nucleation and crystal growth are not sufficient to promote crystallization, and further demonstrates the superior thermal stability of the SCL phases of dyes without alkoxy groups. Contrary to their phenyl analogs, NC5 and NC6 did not exhibit crystallization transitions when cooled rapidly. The slow cooling of NC5 was not sufficient to promote crystallization, but an exothermic peak was observed for NC6 during slow cooling. As with PC12, NC12 exhibits crystallization peaks when cooled rapidly or slowly.

Differential scanning calorimetry results show that the length of the alkoxy chain affects the crystallization dynamics for both phenyl and naphthyl derivatives. As observed in video

characterization, crystallization occurs for dyes with sufficiently long alkoxy chains even during rapid cooling. For phenyl derivatives, PH, PC1, PC3 formed supercooled liquid phases upon rapid cooling, whereas supercooled liquids were observed for naphthyl derivatives with even longer alkyl chains (NH, NC1, NC3, NC5, NC6) when cooled quickly. Reheating dyes resulted in evidence of crystallization for most derivatives, however no transitions were noted for PH and NH with these treatments. While both sets of dyes showed melted states with tunable stability, these results further indicate that naphthyl diketones form more stable supercooled phases than corresponding phenyl dyes.

#### Solid-State Emission

It is clear that packing interactions and other structural effects derived from alkoxy and arene substitution can affect the thermal stability of trimethoxy diketone melted states, however previous studies have shown that these factors also influence the emission of solid-state materials. The degree to which molecular packing affects the properties of solid-state emissive materials is often estimated by comparison of solid and solution emission. In general, when there are fewer dye-dye interactions, the emission of bulk powders is similar to that of their solution spectra. This has been linked to herringbone type packing structures in certain systems. <sup>43</sup> Prior investigation of these effects on BF<sub>2</sub>bdks showed that their solid-state emission blue-shifted as alkyl chain length was increased<sup>23</sup> and redshifted emission was observed for BF<sub>2</sub>bdk dyes with larger arene rings. <sup>44</sup> Given their structural similarities, the solid-state emission of uncoordinated trimethoxy-substituted diketones may exhibit similar trends.

Solid-state optical properties were initially investigated by measuring the emission of powder and melt phases for all dyes. The emission of the melted phase was measured by melting dyes (~10 mg) on a piece of microscope coverglass using a hot plate. The emission of diketones

as bulk powders was compared to their emission in solution in order to gauge the impact of packing on solid-state emission (Table 2). As bulk powders, phenyl dyes glowed blue under UV light, and a narrow range of wavelengths was detected (Figure 7, Figure S8). Slightly higher energy emission was detected for PC3, PC5 and PC12 ( $\lambda_{em}$  = 449 nm) relative to PH ( $\lambda_{em}$  = 458 nm) and PC1 ( $\lambda_{em}$  = 453 nm). Compared to other phenyl dyes, the emission of PC6 ( $\lambda_{em}$  = 480 nm) was more significantly redshifted.

Based on these results no correlation between emission energy and alkoxy chain length can be established. With the exception of PC6, all phenyl derivatives exhibited similar wavelengths between powder and solution. This indicates that most phenyl dyes are packed such that dye-dye interactions have little impact on their solid-state emission. This is consistent with crystal structures obtained for phenyl dyes which showed herringbone-type packing and no  $\pi$ - $\pi$  interactions. However, the peak emission of PC6 is substantially red-shifted compared to solution. Therefore, it is likely that dyes occupy a different packing pattern in PC6 solids. In addition, PC6 exhibited a larger quantum yield (41.6%) compared to other phenyl dyes which also may be the result of different molecular packing.

**Table 2**. Emission Properties of Trimethoxy Substituted Diketones in Solid and Melted States.<sup>a</sup>

	Solid				Melt			
Compound	λem b	$\tau_{\mathrm{pw0}}{}^d$	fwhm <sup>c</sup>	$\Phi_{\mathrm{C}}{}^{e}$	$\lambda_{em}$	$ au_{\mathrm{pw0}}$	$fwhm_{MT}$	$\Phi_{\mathrm{MT}^e}$
Compound	(nm)	(ns)	(nm)	(%)	(nm)	(ns)	(nm)	(%)
PH	458	1.14	62	5.0	505	3.38	126	8.0
PC1	453	0.15	54	5.1	481	6.31	135	10.0
PC3	449	1.25	31	24.0	481	3.76	95	-
PC5	449	1.16	38	23.0	523	5.08	135	-
PC6	480	1.67	52	41.6	481	2.78	114	-
PC12	449	< 0.1	43	24.0	526	2.43	137	-
NH	469	2.56	62	10.9	512	3.06	92	17.0
NC1	458	1.85	59	25.6	497	2.72	100	17.8
NC3	478	0.49	62	12.1	493	1.43	117	8.3
NC5	462	0.91	163	17.3	543	1.76	200	5.4
NC6	470	0.56	57	21.1	498	2.29	112	8.4
NC12	486	0.70	99	4.8	535	3.24	152	-

<sup>a</sup> Excited at 369 nm, room temperature, air. <sup>b</sup> Emission maximum. <sup>c</sup> Full width at half maximum. <sup>d</sup> Pre-exponential weighted lifetime. <sup>e</sup> Quantum yield measured using crystalline (C) and melted (MT) glass films

In most cases, the emission of naphthyl derivatives as powders was red-shifted compared to their corresponding phenyl dyes. However, PC6 powders emitted lower energy photons compared to all naphthyl dyes with the exception of NC12 ( $\lambda_{em}$  = 486 nm). While NC12 and NC1 ( $\lambda_{em}$  = 458 nm) exhibited the lowest and highest energy emission detected for naphthyl dyes, respectively, the emission of NC3 was significantly red-shifted compared to derivatives with alkyl chains of intermediate length (NC5 and NC6). Like their phenyl counterparts, this demonstrates that there is no trend in solid-state emission with increasing alkoxy chain length for naphthyl dyes.

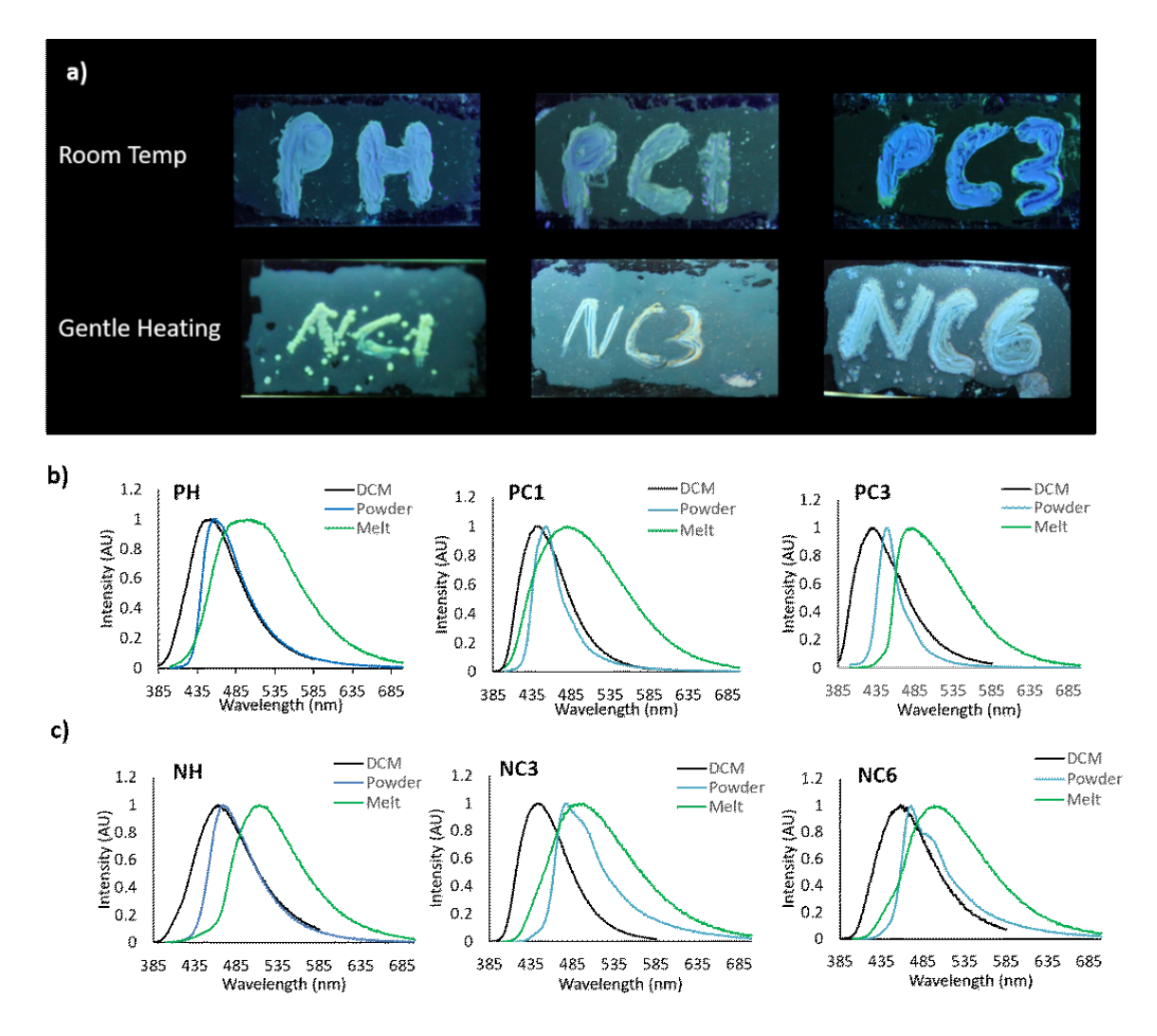


**Figure 7**. Images under UV irradiation of mechanically perturbed melted phenyl dye thin films (a). Emission spectra of selected phenyl (b) and naphthyl (c) dyes in dichloromethane solution, as pristine powders, and as melted films.

All dyes in the melted phase, regardless of arene substitution, glowed green under UV irradiation, however a wider range of emission wavelengths was detected compared to their corresponding bulk powders. For phenyl dyes, the bluest emission was observed for PC1, PC3, and PC6 ( $\lambda_{em} = 481$  nm) whereas PC12 exhibited the most redshifted melt ( $\lambda_{em} = 526$  nm). Naphthyl dyes exhibited different behavior, where the highest energy emission was noted for NC3 ( $\lambda_{em} = 493$  nm), and NC5 ( $\lambda_{em} = 543$  nm) was the most red-shifted. Additionally, broad emission profiles were observed in NC5 and NC6 samples. This may be due to multiple emissive species.<sup>27</sup>

As with their powder emission, no trends in emission wavelength of the melted phase with increasing chain length were detected for phenyl or naphthyl dyes. However, overlapping emission wavelengths were observed between phenyl and naphthyl derivatives which indicates that increasing arene size does not necessarily correspond to redshifted emission, as was the case for bulk powders. These results indicate that the emission of the melted phase cannot be systematically tuned through these methods.

As depicted in the video characterization of phenyl dyes, mechanical shearing of certain phenyl dyes resulted in localized crystallization at room temperature. With the exception of NC6, the same shearing induced crystallization at room temperature was not observed in naphthyl dyes. However, gentle heating of mechanically perturbed melted phases of naphthyl dyes induced localized crystallization for these derivatives. The contrast between these states can be analyzed using their quantum yields ( $\phi$ ) (Table 2). The quantum yields for all derivatives were measured in the crystalline phase, however obtaining quantum yields for melts was limited by melt phase thermal stability. Therefore, quantum yields in the melted state were not measured for PC5, PC6, PC12, and NC12 due to rapid crystallization.

In the crystalline state, the quantum yield of phenyl dyes can be tuned through alkoxy substitution. The lowest quantum yields were observed for PH and PC1, but increased quantum yields were observed for dyes with longer chain lengths before reaching a maximum for PC6 ( $\Phi_C$  = 41.6 %). As observed for iodo-substituted BF<sub>2</sub>bdk dyes with varying length alkoxy groups in solution, this observation may be due to greater anchoring of the alkoxy substituted phenyl ring in dyes substituted with longer chains, which hinders rotation.<sup>24</sup> For naphthyl dyes, the quantum yield fluctuates as the alkoxy substituent was increased. In the melted state, little deviation in quantum yield was observed between PH and PC1, however the quantum yield diminished for naphthyl

dyes as the alkoxy chain was increased above a single carbon. Compared to the crystalline state, PH and PC1 exhibited higher quantum yields in the melted state whereas all naphthyl but NC1 exhibited larger quantum yields in the crystalline state. According to the differences in quantum yield, NC6 shows the highest contrast upon shear induced crystallization.

#### Mechanochromic Luminescence

Unlike the mechanically induced crystallization properties described above, the mechanochromic luminescent (ML) properties of bdk and BF<sub>2</sub>bdk dyes typically involve a redshift in emission that is the result of a crystalline-to-amorphous phase transition. Previously, PC1 showed blue-to-green ML with rapid self-erasing ( $\sim 30 \text{ s} - 5 \text{ min}$ , depending on the sample). To test the ML properties of phenyl and naphthyl derivatives, spin-cast films were prepared with dilute (0.18 M) dye solutions in dichloromethane. The emission of each film was measured in as spun (AS), thermally annealed (TA) and smeared (SM) states (Table 3). In general, phenyl dyes were annealed at 75 °C for 10 minutes to produce films in the TA state. With the exception of PH and PC1, this was sufficient to produce a crystalline phase with maximally blue-shifted emission. To anneal PH and PC1, films were smeared with a Kimwipe by applying gentle pressure to the sample and rubbing in a single direction before subsequent heating at 75 °C for another 10 minutes. For all naphthyl dyes but NC12, films were heated at 85 °C for 10 minutes, followed by gentle smearing with a Kimwipe and additional heating at 85 °C for another 10 minutes to make TA films. The smearing and reheating step was omitted for NC12 as blue-shifted emission was observed after heating at 85 °C for only 10 min.

**Table 3**. Optical Properties of SCLs on Glass.<sup>a</sup>

	As Spun		Annealed		Sm	neared
Compound	$\lambda_{\mathrm{em}}{}^{b}$	$fwhm^c$	$\lambda_{\text{em}}$	fwhm	$\lambda_{em}$	fwhm
Compound	(nm)	(nm)	(nm)	(nm)	(nm)	(nm)
PH	471	102	470	106	496	103
PC1	499	141	428	35	478	122
PC3	441	36	441	36	474	37
PC5	432	38	434	37	477	106
PC6	451	72	452	56	476	50
PC12	445	60	445	59	481	86
NH	484	111	467	72	480	105
NC1	485	114	485	114	501	111
NC3	480	111	468	80	483	107
NC5	470	138	457	71	486	134
NC6	478	108	483	114	487	111
NC12	476	99	470	101	446	83

<sup>&</sup>lt;sup>a</sup> Excited at 369 nm, room temperature, air. <sup>b</sup> Emission maximum. <sup>c</sup> Full width at half maximum.

With the exception of PH and PC1, films glowed blue in the AS state (Figure 8, Figure S9). Green emission was observed for PH ( $\lambda_{em}$  = 471 nm) and PC1 ( $\lambda_{em}$  = 471 nm). The differences observed in PH and PC1 are in accordance with XRD and DSC studies and indicate that dyes substituted with longer alkoxy chains have a greater propensity to crystallize. No trend in emission wavelength with alkoxy chain length was observed for AS films of blue emissive dyes, as PC3 ( $\lambda_{em}$  = 441 nm) exhibited the maximally blue-shifted emission and the lowest energy emission was observed for PC6 ( $\lambda_{em}$  = 451 nm). Thermal annealing of phenyl dye films resulted in a large blue-shift for PC1, however little change in emission was observed for all other phenyl dyes, which indicates that they are likely crystalline in the AS phase. The emission of PH bulk powder ( $\lambda_{em}$  = 458 nm), suggests that higher energy emission should be achievable, however annealing and gently smearing was insufficient to produce blue emission. For all phenyl dyes but PC6, the peak emission of annealed films is similar (< 5 nm) to the emission of monomer in dichloromethane which

suggests that dye-dye interactions that modulate emission are very weak or absent for annealed films. The peak emission of PC6 is redshifted relative to emission in dichloromethane, therefore interactions between PC6 molecules are likely present in these films.

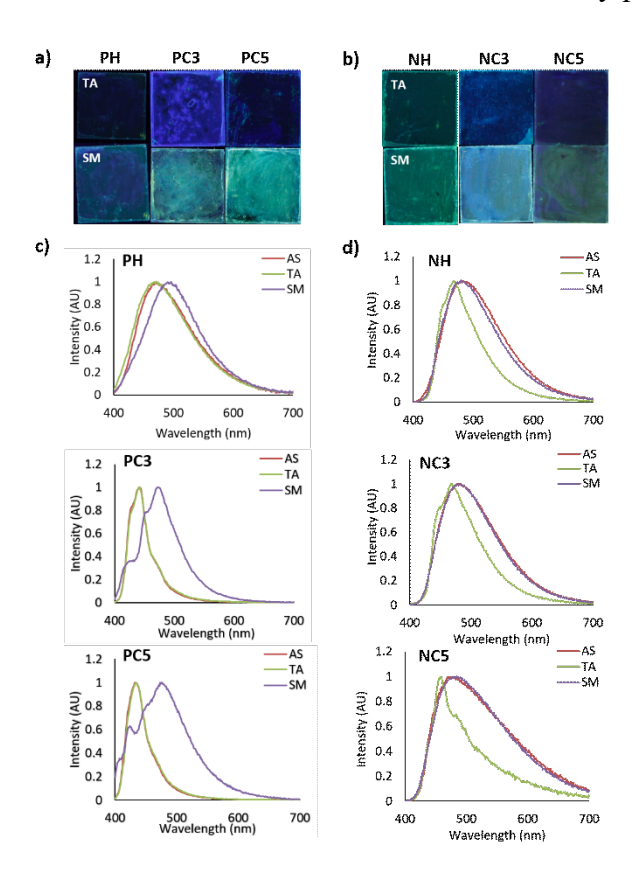


**Figure 8**. Images under UV irradiation of thermally annealed (TA) and smeared (SM) thin films of phenyl (a) and naphthyl dyes. Normalized emission spectra of selected phenyl (c) and naphthyl (d) dye films in as spun (AS), TA and SM states.

Smearing resulted in redshifted emission for all dyes, however the extent of ML shift was highly dependent on alkoxy chain length. The ML shifts ( $\Delta\lambda_{ML}$ ) varied depending on alkoxy chain length, however no clear trend could be established. The smallest ML shifts were observed for PH and PC6 ( $\Delta\lambda_{ML}$  < 26 nm) and the largest ML shifts for phenyl dyes were observed in PC1 and PC5 ( $\Delta\lambda_{ML}$  > 43 nm). With the exception of PC1, no evidence of self-erasing was observed for phenyl dyes 24 hours after smearing, which indicates that room temperature recovery is hindered in

derivatives with longer alkoxy chains. The same trend was observed in BF<sub>2</sub>bdk dyes with differing alkoxy chains.

For films of naphthyl dyes, the AS state glowed green under UV irradiation. Compared to phenyl dyes, broader emission profiles were observed regardless of alkoxy chain length. Thermal annealing of naphthyl films resulted in very little change in peak emission for NC1 and NC6. Relatively small changes in peak wavelength were observed compared to phenyl dyes, however there were substantial reductions in full width at half maxima (fwhm), especially for NH, NC3, NC5 and NC12. With the exception of NH, which showed similar peak emission with respect to dichloromethane solutions, large deviations in peak emission between solution and solid state spectra were observed for naphthyl dyes. This is indicative of more significant intermolecular interactions between dyes for all alkoxy substituted naphthyl dyes. With the exception of NC5, changes in peak emission and spectral broadening were observed for naphthyl dyes indicating ML activity. No evidence of room temperature self-recovery was observed for naphthyl dyes. Much smaller ML shifts and lower contrast emission changes were detected in comparison to phenyl derivatives.

#### Conclusions

Based on video characterization as well as DSC and powder XRD results, all dyes formed supercooled liquid phases when melted and cooled in air. The thermal stability of trimethoxy-substituted diketone SCL phases could be tuned using a combination of alkoxy chain length and arene effects. In general, naphthyl SCLs exhibited greater thermal stability than phenyl counterparts. Additionally, dyes substituted with longer alkoxy chains exhibited faster crystallization compared to unsubstituted derivatives or dyes with shorter chains. For certain derivatives, mechanically induced crystallization was observed at room temperature (PH, PC1,

PC3 and NC6). Single crystal analysis of selected phenyl derivatives indicated that the parasubstituted methoxy groups of the trimethoxy rings were out of the molecular plane. Furthermore, the torsion angles of these methoxy groups correlated with the thermal stability of the melted phase. For the most part, dyes that exhibited smaller torsion angles showed lower thermal stability of the melted phase (i.e. faster conversion to the crystalline state). This was attributed to diminished steric interactions preventing crystallization.

The optical properties were also dependent on arene substitution, as the crystalline phases of naphthyl dyes were redshifted compared to phenyl derivatives. No trends could be established with increasing alkoxy chain length for either the phenyl and naphthyl sets. Mechanochromic luminescence was also observed for most derivatives. While dyes exhibited blue-to-green emission changes upon mechanical perturbation, the degree of wavelength shift was dependent on alkoxy chain length. These results indicate that certain trimethoxy derivatives exhibit two types of mechanochromic luminescence at room temperature; namely, (a) traditional ML, where an amorphous state with redshifted emission is generated from an initial blue shifted crystalline phase, and (b) shear induced crystallization, where mechanical disruption of a supercooled liquid phase results in brighter blue-shifted emission.

#### **Associated Content**

Supporting Information

The supporting information is free of charge on the ACS Publications website. Synthesis and <sup>1</sup>H NMR spectral data of all new compounds, absorption and emission spectra in dichloromethane, powder X-ray diffraction patterns, crystal structure views, emission spectra of single crystals, differential scanning calorimetry (DSC) thermograms, normalized emission spectra of phenyl and

naphthyl dyes in dichloromethane solutions, as prepared powders, and as melted films, and normalized emission spectra of phenyl and naphthyl dyes as thin films in the as spun (AS), thermally annealed (TA), and smeared (SM) states (PDF). Crystallographic information file

describing single crystal and molecular packing of PH (CIF), PC3 (CIF), and PC5 (CIF)

**Author Information** 

Corresponding Author

\*E-mail: fraser@virginia.edu

Notes

The authors declare no competing financial interest.

Acknowledgements

We thank the National Science Foundation (CHE-1213915 and CHE-1709322) and the University of Virginia Department of Chemistry for support for this research.

References

(1) Jiang, Y. An Outlook Review: Mechanochromic Materials and Their Potential for Biological and Healthcare Applications. *Mater. Sci. Eng. C* **2014**, *45*, 682–689.

(2) Zhang, X.; Chi, Z.; Zhang, Y.; Liu, S.; Xu, J. Recent Advances in Mechanochromic

Luminescent Metal Complexes. J. Mater. Chem. C 2013, 1, 3376–3390.

Sagara, Y.; Yamane, S.; Mitani, M.; Weder, C.; Kato, T. Mechanoresponsive Luminescent (3)

Molecular Assemblies: An Emerging Class of Materials. Adv. Mater. 2016, 28, 1073–

1095.

**(4)** Sagara, Y.; Kato, T. Mechanically Induced Luminescence Changes in Molecular

35

- Assemblies. Nat. Chem. 2009, 1, 605–610.
- (5) Ma, Z.; Teng, M.; Wang, Z.; Yang, S.; Jia, X. Mechanically Induced Multicolor Switching Based on a Single Organic Molecule. *Angew. Chemie Int. Ed.* **2013**, *52*, 12268–12272.
- (6) Ito, H.; Saito, T.; Oshima, N.; Kitamura, N.; Ishizaka, S.; Hinatsu, Y.; Wakeshima, M.; Kato, M.; Tsuge, K.; Sawamura, M. Reversible Mechanochromic Luminescence of [(C6F 5Au)2(μ-1,4-Diisocyanobenzene)]. J. Am. Chem. Soc. 2008, 130, 10044–10045.
- (7) Zhang, G.; Lu, J.; Sabat, M.; Fraser, C. L. Polymorphism and Reversible Mechanochromic Luminescence for Solid-State Difluoroboron Avobenzone. *J. Am. Chem. Soc.* 2010, 132, 2160–2162.
- (8) Ito, H.; Muromoto, M.; Kurenuma, S.; Ishizaka, S.; Kitamura, N.; Sato, H.; Seki, T. Mechanical Stimulation and Solid Seeding Trigger Single-Crystal-to-Single-Crystal Molecular Domino Transformations. *Nat. Commun.* 2013, 4, 2009.
- (9) Yagai, S.; Seki, T.; Aonuma, H.; Kawaguchi, K.; Karatsu, T.; Okura, T.; Sakon, A.; Uekusa, H.; Ito, H. Mechanochromic Luminescence Based on Crystal-to-Crystal Transformation Mediated by a Transient Amorphous State. *Chem. Mater.* 2016, 28, 234–241.
- (10) Seki, T.; Takamatsu, Y.; Ito, H. A Screening Approach for the Discovery of Mechanochromic Gold(I) Isocyanide Complexes with Crystal-to-Crystal Phase Transitions. J. Am. Chem. Soc. 2016, 138, 6252–6260.
- (11) Chung, K.; Kwon, M. S.; Leung, B. M.; Wong-Foy, A. G.; Kim, M. S.; Kim, J. J.; Takayama, S.; Gierschner, J.; Matzger, A. J.; Kim, J. J. Shear-Triggered Crystallization and Light Emission of a Thermally Stable Organic Supercooled Liquid. *ACS Cent. Sci.* 2015, 1, 94–102.

- (12) Hancock, B. C.; Parks, M. What Is the True Solubility Advantage for Amorphous Pharmaceuticals? *Pharm. Res.* **2000**, *17*, 397–404.
- (13) Karasawa, S.; Hagihara, R.; Abe, Y.; Harada, N.; Todo, J.; Koga, N. Crystal Structures,
  Thermal Properties, and Emission Behaviors of N, N R-Phenyl-7-Amino-2,4-Tri Fl
  Uoromethylquinoline Derivatives: Supercooled Liquid-to-Crystal Transformation Induced by Mechanical Stimuli. *Cryst. Growth Des.* **2014**, *14*, 2468–2478.
- (14) Shirota, Y. Photo- and Electroactive Amorphous Molecular Materials-Molecular Design, Syntheses, Reactions, Properties, and Applications. *J. Mater. Chem.* **2005**, *15*, 75–93.
- (15) Shirota, Y.; Kageyama, H. Charge Carrier Transporting Molecular Materials and Their Applications in Devices Charge Carrier Transporting Molecular Materials and Their Applications in Devices. *Chem. Rev.* 2007, 107, 953–1010.
- (16) Ren, Y.; Lee, J.; Hutchins, K. M.; Sottos, N. R.; Moore, J. S. Crystal Structure, Thermal Properties, and Shock-Wave-Induced Nucleation of 1,2-Bis(phenylethynyl)benzene.

  Cryst. Growth Des. 2016, 16, 6148–6151.
- (17) Hariharan, P. S.; Moon, D.; Anthony, S. P. Crystallization-Induced Reversible Fluorescence Switching of Alkyl Chain Length Dependent Thermally Stable Supercooled Organic Fluorescent Liquids. *CrystEngComm* 2017, 19, 6489–6497.
- (18) Stillinger, F. H. A Topographic View of Supercooled Liquids and Glass Formation. *Science* **1995**, *267*, 1935–1939.
- (19) Debenedetti, P. G. *Metastable Liquids: Concepts and Principles*; Princeton University Press: Princeton, N. J., 1996.
- (20) Whitaker, C. M.; McMahon, R. J. Synthesis and Characterization of Organic Materials with Conveniently Accessible Supercooled Liquid and Glassy Phases: Isomeric 1,3,5-

- Tris(naphthyl)benzenes. J. Phys. Chem. 1996, 100, 1081–1090.
- (21) Butler, T.; Morris, W. A.; Samonina-Kosicka, J.; Fraser, C. L. Mechanochromic Luminescence and Aggregation Induced Emission for a Metal-Free β-Diketone. *Chem. Commun.* 2015, 51, 3359–3362.
- (22) Butler, T.; Morris, W. A.; Samonina-Kosicka, J.; Fraser, C. L. Mechanochromic Luminescence and Aggregation Induced Emission of Dinaphthoylmethane β-Diketones and Their Boronated Counterparts. *ACS Appl. Mater. Interfaces* **2016**, *8*, 1242–1251.
- (23) Nguyen, N. D.; Zhang, G.; Lu, J.; Sherman, A. E.; Fraser, C. L. Alkyl Chain Length Effects on Solid-State Difluoroboron β-Diketonate Mechanochromic Luminescence. *J. Mater. Chem.* **2011**, *21*, 8409–8415.
- (24) Morris, W. A. W. A.; Sabat, M.; Butler, T.; Derosa, C. A.; Fraser, C. L. Modulating Mechanochromic Luminescence Quenching of Alkylated Iodo Difluoroboron Dibenzoylmethane Materials. J. Phys. Chem. C 2016, 120, 14289–14300.
- (25) Wang, F.; Song, D.; Dickie, D. A.; Fraser, C. L. Ring Size Effects on Multi-Stimuli Responsive Luminescent Properties of Cyclic Amine Substituted β-Diketones and Difluoroboron Complexes. *Chem. Asian J.* **2019**, *14*, 1849–1859.
- (26) Zhang, G.; Lu, J.; Fraser, C. L. Mechanochromic Luminescence Quenching: Force-Enhanced Singlet-to-Triplet Intersystem Crossing for Iodide-Substituted Difluoroboron–Dibenzoylmethane–Dodecane in the Solid State. *Inorg. Chem.* 2010, 49, 10747–10749.
- (27) Morris, W. A.; Liu, T.; Fraser, C. L. Mechanochromic Luminescence of Halide-Substituted Difluoroboron β-Diketonate Dyes. *J. Mater. Chem. C* **2015**, *3*, 352–363.
- (28) Butler, T.; Wang, F.; Fraser, C. L. Controlling Solid-State Optical Properties of Stimuli

- Responsive Dimethylamino-Substituted Dibenzoylmethane Materials. *Mater. Chem. Front.* **2017**, *1*, 1804–1817.
- (29) Wang, F.; DeRosa, C. A.; Daly, M. L.; Song, D.; Sabat, M.; Fraser, C. L. Multi-Stimuli Responsive Luminescent Azepane-Substituted β-Diketones and Difluoroboron Complexes. *Mater. Chem. Front.* **2017**, *1*, 1866–1874.
- (30) Morris, W. A.; Butler, T.; Kolpaczynska, M.; Fraser, C. L. Stimuli Responsive Furan and Thiophene Substituted Difluoroboron β-Diketonate Materials. *Mater. Chem. Front.* 2017, 1, 158–166.
- (31) Morris, W. A.; Kolpaczynska, M.; Fraser, C. L. Effects of α-Substitution on Mechanochromic Luminescence and Aggregation-Induced Emission of Difluoroboron β-Diketonate Dyes. J. Phys. Chem. C 2016, 120, 22539–22548.
- (32) Butler, T.; Mathew, A. S.; Sabat, M.; Fraser, C. L. Camera Method for Monitoring a Mechanochromic Luminescent β-Diketone Dye with Rapid Recovery. *ACS Appl. Mater. Interfaces* **2017**, *9*, 17603–17612.
- (33) Williams, D. B. G.; Lawton, M. Drying of Organic Solvents: Quantitative Evaluation of the Efficiency of Several Desiccants. *J. Org. Chem.* **2010**, *75*, 8351–8354.
- (34) Zhang, G.; Evans, R. E.; Campbell, K. A.; Fraser, C. L. Role of Boron in the Polymer Chemistry and Photophysical Properties of Difluoroboron–Dibenzoylmethane Polylactide. *Macromolecules* 2009, 42, 8627–8633.
- (35) Hubaud, J.-C. C.; Bombarda, I.; Decome, L.; Wallet, J.-C. C.; Gaydou, E. M. Synthesis and Spectroscopic Examination of Various Substituted 1,3-Dibenzoylmethane, Active Agents for UVA/UVB Photoprotection. *J. Photochem. Photobiol. B Biol.* **2008**, *92*, 103–109.

- (36) Demas, J. N.; Crosby, G. A. The Measurement of Photoluminescence Quantum Yields. A Review. *J. Phys. Chem.* **1971**, *75*, 991–1024.
- (37) Zhu, H.; Wang, X.; Li, Y.; Wang, Z.; Yang, F.; Yang, X. Microwave Synthesis of Fluorescent Carbon Nanoparticles with Electrochemiluminescence Properties. *Chem. Commun.* **2009**, *0*, 5118–5120.
- (38) Chow, Y. L.; Johansson, C. I.; Zhang, Y.-H.; Gautron, R.; Yang, L.; Rassat, A.; Yang, S.-Z. Spectroscopic and Electrochemical Properties of 1,3-Diketonatoboron Derivatives. *J. Phys. Org. Chem.* 1996, 9, 7–16.
- (39) DeRosa, C. A.; Kerr, C.; Fan, Z.; Kolpaczynska, M.; Mathew, A. S.; Evans, R. E.; Zhang, G.; Fraser, C. L. Tailoring Oxygen Sensitivity with Halide Substitution in Difluoroboron Dibenzoylmethane Polylactide Materials. ACS Appl. Mater. Interfaces 2015, 7, 23633–23643.
- (40) Samonina-Kosicka, J.; DeRosa, C. A.; Morris, W. A.; Fan, Z.; Fraser, C. L. Dual-Emissive Difluoroboron Naphthyl-Phenyl β-Diketonate Polylactide Materials: Effets of Heavy Atom Placement and Polymer Molecular Weight. *Macromolecules* **2014**, *47*, 3736–3746.
- (41) Barsoum, M. W. Fundamentals of Ceramics; CRC Press: Boca Raton, FL, 2002.
- (42) Debenedetti, P. G.; Stillinger, F. H. Supercooled Liquids and the Glass Transition. *Nature* **2001**, *410*, 259–267.
- (43) Varghese, S.; Das, S. Role of Molecular Packing in Determining Solid-State Optical
   Properties of π-Conjugated Materials. J. Phys. Chem. Lett 2011, 2, 863–873.
- (44) Liu, T.; Chien, A. D.; Lu, J.; Zhang, G.; Fraser, C. L. Arene Effects on Difluoroboron β-Diketonate Mechanochromic Luminescence. J. Mater. Chem. 2011, 21, 8401–8408.

## Table of Contents Graphic

## Shear Induced Crystallization

